

## Side-surface-mediated hybridization in axion insulators

Rui Chen,<sup>1,\*</sup> Hai-Peng Sun<sup>2,†</sup> and Bin Zhou<sup>1,‡</sup>

<sup>1</sup>*Department of Physics, Hubei University, Wuhan 430062, China*

<sup>2</sup>*Institute for Theoretical Physics and Astrophysics, University of Würzburg, 97074 Würzburg, Germany*



(Received 20 November 2022; revised 19 February 2023; accepted 27 February 2023; published 10 March 2023)

The axion insulator is believed to host half-quantized chiral currents running antiparallely on its top and bottom surfaces. However, the experimental detection of the half quantization in axion insulators remains elusive. In this paper, we propose a mechanism to explain why the half quantization is hard to be probed by showing that the half-quantized counterpropagating currents in axion insulator thin films are strongly suppressed due to the hybridization mediated by the massless side-surface states. This side-surface-mediated hybridization leads to a different type of finite-size effect, which features a power-law decay with the increasing film thickness, different from the exponential decay in topological insulators. Moreover, we show that the half quantization can be extracted in the axion insulator phase by adopting the nonlocal transport measurement.

DOI: [10.1103/PhysRevB.107.125304](https://doi.org/10.1103/PhysRevB.107.125304)

### I. INTRODUCTION

The axion insulator is characterized by a symmetry-protected quantized axion coupling coefficient [1–5], which shares the half-quantized surface Hall conductance [6–9] and a unique topological magnetoelectric effect [10–15]. The bulk-boundary correspondence implies the existence of topologically protected half-quantized hinge currents in the axion insulator. Many efforts have been devoted towards the search for half quantization in the axion insulator in various magnetic topological materials, including magnetically doped topological insulators [16–25] and intrinsic antiferromagnetic topological insulators [26–32]. The detection of half quantization is important because it provides evidence for not only the surface Hall effect but also the long-sought axion insulator phase.

The heterostructures of a magnetically doped topological insulator and intrinsic antiferromagnetic topological insulator have been proposed to host an axion insulator phase [19–21,29,30], which is characterized by an intermediate zero Hall conductance plateau. Nevertheless, this is still in debate [17,28,33], since a normal insulator also manifests the zero Hall conductance plateau [5]. So far, there is no transport signature for a half-quantized counterpropagating current in the axion insulator phase. Therefore, the search for transport signatures of half quantization in the axion insulator phase is still an open problem.

In this paper, we investigate the transport in magnetic topological insulators by adopting a four-terminal Hall-bar setup. We reveal the existence of half-quantized counterpropagating currents in the axion insulator phase. Surprisingly, we find that the half-quantized counterpropagating currents are strongly

suppressed in thin films. This can be attributed to the massless side-surface states that bridge the counterpropagating currents on the top and bottom surfaces. Moreover, this strong effect is characterized by a power-law decay of the hybridization gap as the film thickness increases. This scenario is distinct from the finite-size effect in other topological materials [34–37], where the boundary states are hybridized via a fully gapped bulk and the hybridization gap exhibits an exponential decay while increasing the system size.

This paper is organized as follows. In Sec. II, we present a tight-binding Hamiltonian for a three-dimensional magnetic topological insulator. In Sec. III, the method of extracting half quantization from the nonlocal transport and the influence of the hybridization on transport properties are demonstrated. In Sec. IV, the power-law decay behavior of the hybridization is studied by numerical calculations. In Sec. V, the physical picture of the hybridization is revealed by an effective model analysis. Finally, the conclusion and discussion are given in Sec. VI.

### II. MODEL

To carry out numerical studies on the magnetic topological insulator, we consider a tight-binding Hamiltonian on a cubic lattice for an isotropic three-dimensional magnetic topological insulator [16,17,38,39],

$$\mathcal{H} = \sum_i c_i^\dagger \mathcal{M}_0 c_i + \sum_{i,\alpha=x,y,z} (c_i^\dagger \mathcal{T}_\alpha c_{i+\alpha} + c_{i+\alpha}^\dagger \mathcal{T}_\alpha^\dagger c_i), \quad (1)$$

where  $\mathcal{T}_\alpha = B\sigma_0\tau_z - i\frac{A}{2}\sigma_\alpha\tau_x$  and  $\mathcal{M}_0 = (M - 6B)\sigma_0\tau_z + m(z)\sigma_z\tau_0$  with the lattice space taken to be unity. Near the  $\mathbf{k} = \mathbf{0}$  point in the momentum space (i.e., the low-energy regime), this model is reduced to a Dirac-like model in the absence of magnetization [ $m(z) = 0$ ]. When magnetization is introduced to a certain surface, its massless Dirac cone opens an energy gap characterized by half-quantized Hall conductance with its sign depending on the magnetization

\*chenr@hubu.edu.cn

†haipeng.sun@physik.uni-wuerzburg.de

‡binzhou@hubu.edu.cn

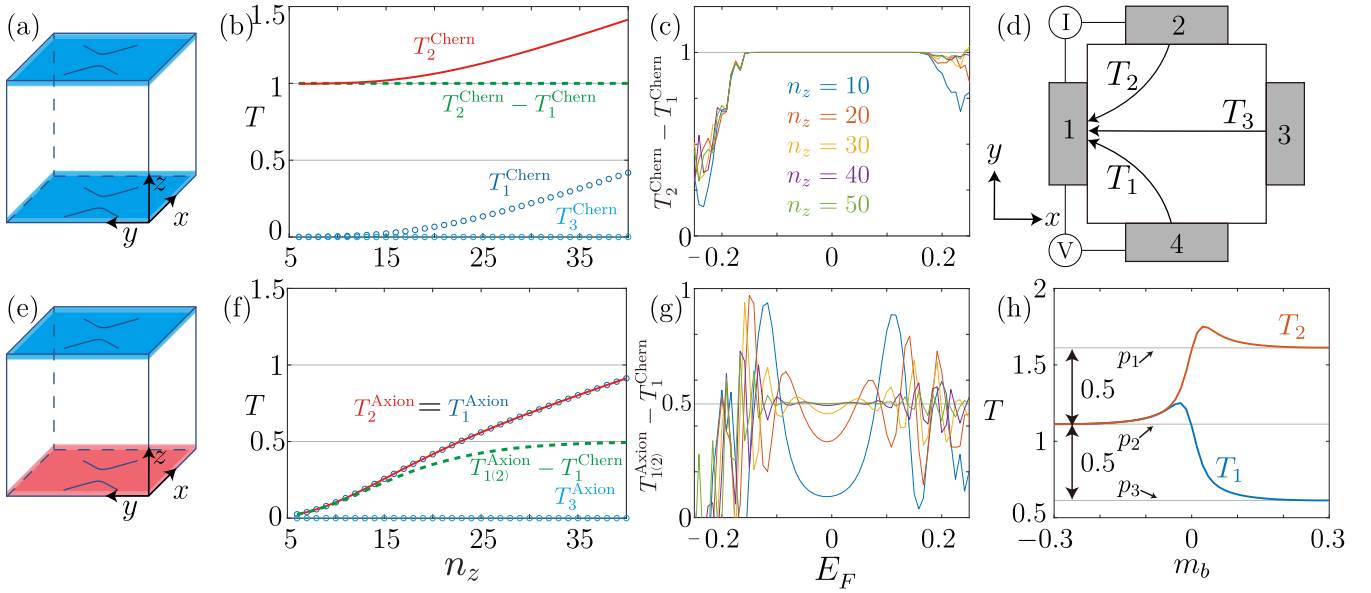


FIG. 1. (a) Schematic illustration of the Chern insulator phase in a magnetic topological insulator. Each of the magnetic top and bottom surfaces hosts a gapped Dirac cone characterized by a half-quantized Hall conductance. (b), (c) Numerically calculated transmission coefficients as functions of (b) the thickness  $n_z$  with  $E_F = 0.01$  and (c) Fermi energy  $E_F$  with different film thicknesses  $n_z$ . The system size is taken as  $n_x = n_y = 30$ . The magnetization strength for the Chern insulator phase is taken as  $m_t = m_b = 0.15$ . Here,  $T_1$ ,  $T_2$ , and  $T_3$  are the transmission coefficients between two clockwise neighboring, counterclockwise neighboring, and non-neighboring terminals, respectively. (d) Schematic illustration of the four-terminal Hall-bar setup.  $T_{1,2,3}$  can be obtained through the nonlocal transport. (e)–(g) The same as (b)–(c) except that they depict the axion insulator phase with  $m_t = -m_b = 0.15$ . The superscripts “Chern” in (b) and “Axion” in (f) are to distinguish the Chern and axion insulator phases, respectively. (h) The transmission coefficients as functions of  $m_b$ , where we take  $m_t = 0.15$ . The system size is taken as  $n_x = n_y = 30$  and  $n_z = 50$ .

direction. The magnetic effect is represented by layer-dependent magnetization that acts as an effective Zeeman field  $m(z)$ . We consider two different cases: the Chern insulator phase and axion insulator phase. We take  $m(z) = m_b$  for  $z = 1, 2$ ,  $m(z) = m_t$  for  $z = n_z - 1, n_z$  and  $m(z) = 0$  elsewhere. As illustrated in Figs. 1(a) and 1(e), we have  $m_t m_b > 0$  ( $m_t m_b < 0$ ) for the Chern (axion) insulator phase. For both Chern and axion insulator phases, the magnetization is introduced to the top and bottom surfaces, and therefore the spectra of surface states open energy gaps at the  $\Gamma$  point on both the top and bottom surfaces [Figs. 1(a) and 1(e)]. For the Chern insulator phase with parallel magnetization alignment on the top and bottom surfaces, the two energy gaps are characterized by half-quantized Hall conductance [10,40,41] with the same sign, and they combine to yield a quantized Hall conductance (see Sec. SII of the Supplemental Material [42] and Refs. [10,16,28,37,40,41,43–55] therein). The top and bottom surfaces with antiparallel magnetization alignment are characterized by half-quantized Hall conductances with opposite signs on each surface, which leads to the emergence of the axion insulator phase. In the numerical calculations, we take the parameters as  $A = 0.5$ ,  $B = 0.25$ , and  $M = 0.4$ .

### III. TRANSPORT SIGNATURES

We investigate the transport signatures of the axion and Chern insulator phases in a four-terminal Hall-bar setup as shown in Fig. 1(d). From the Landauer-Büttiker formula at zero temperature, the current flowing into terminal  $p$  is given by  $I_p = \frac{e^2}{h} \sum_{q \neq p} T_{pq}(E_F)(V_p - V_q)$  [43,44].  $T_{pq}$  depicts the

transmission coefficient from electrode  $q$  to  $p$ .  $V_i$  corresponds to the voltage of lead  $i$  shown in Fig. 1(d). The transmission matrix is found to have the following form in numerical calculations,

$$T = \begin{pmatrix} 0 & T_1 & T_3 & T_2 \\ T_2 & 0 & T_1 & T_3 \\ T_3 & T_2 & 0 & T_1 \\ T_1 & T_3 & T_2 & 0 \end{pmatrix}, \quad (2)$$

where  $T_1$  and  $T_2$  are the clockwise and anticlockwise transmission coefficients between two neighboring terminals, respectively, and  $T_3$  is the transmission coefficient between two non-neighboring terminals, as shown in Fig. 1(d). The diagonal terms represent the reflection of charge carriers within the same terminal, and only depend on the matching between the terminals and conductors. These terms are irrelevant to the intrinsic properties of the material. Therefore, we assume the diagonal terms of the transmission matrix to be zero for simplicity. It is noticed that the magnetic topological insulator thin film can be regarded as a quasi-two-dimensional (2D) system with an insulating bulk and conducting edge channels. Electrons can only propagate from one terminal to the next-neighboring terminal along the “edge” of the quasi-2D system. Thus, only the transmission coefficients between two neighboring terminals are nonzero.

Figure 1(b) shows the transport coefficients of the Chern insulator phase as functions of the film thickness  $n_z$ . It is the difference between the clockwise and counterclockwise channels (i.e.,  $T_2^{\text{Chern}} - T_1^{\text{Chern}}$ ) that characterizes the Chern

insulator phase with  $T_1^{\text{Chern}}$  being the contributions from side surfaces. For thin films, we notice that  $T_{1(3)}^{\text{Chern}} = 0$  and  $T_2^{\text{Chern}} = 1$ , which indicates that only the chiral currents on the top and bottom surfaces contribute to the transport. For thick films,  $T_{1(2)}^{\text{Chern}}$  increase with increasing film thickness due to the increasing conducting channels from the side surfaces. But the chiral difference  $T_2^{\text{Chern}} - T_1^{\text{Chern}} = 1$  remains quantized, which establishes the Chern insulator phase [Fig. 1(c)].

Figure 1(f) shows the transport coefficients of the axion insulator phase as functions of the film thickness  $n_z$ . We observe  $T_1^{\text{Axion}} = T_2^{\text{Axion}}$ , which indicates the vanishing of the net chiral current and agrees well with the magnetic compensated nature of axion insulators. Due to the contributions of side surfaces,  $T_{1(2)}^{\text{Axion}}$  increases with increasing film thickness  $n_z$ . We calculate  $T_{1(2)}^{\text{Axion}} - T_2^{\text{Chern}}$  as a function of  $n_z$ . For thick films,  $T_{1(2)}^{\text{Axion}} - T_1^{\text{Chern}} = 1/2$ , indicating that the system corresponds to an axion insulator with a half-quantized counterpropagating current. For thin films, the half-quantized counterpropagating current is strongly suppressed. The hybridization effect in the axion insulator phase can be observed more clearly in Fig. 1(g).

In experiments,  $T_1$ ,  $T_2$ , and  $T_3$  can be measured through the nonlocal measurement [28,48,49] by adopting the four-terminal Hall-bar setup [see Fig. 1(d) and Sec. SI of the Supplemental Material [42] for more details]. The axion and Chern insulator phases can be tuned by applying an external magnetic field [1,20,21,56]. To simulate this process, we consider a more general case with a fixed  $m_t = 0.15$  and a varying  $m_b$ . Figure 1(h) illustrates the transmission coefficients  $T_1$  and  $T_2$  as functions of  $m_b$ , which shows three plateaus with the values  $p_1 = 1.61$ ,  $p_2 = 1.11$ , and  $p_3 = 0.61$ . For  $m_b > 0$ , the Chern insulator phase is characterized by the difference  $p_1 - p_3 = 1$ . On the other hand, for  $m_b < 0$ , the axion insulator phase is identified by  $p_1 - p_2 = p_2 - p_3 = 0.5$ . This scenario offers the possibility of experimentally detecting the half-quantized counterpropagating chiral currents in axion insulators and is able to distinguish axion insulators from normal insulators. Near the critical value  $m_b = 0$ , the shift of  $T_1$  and  $T_2$  from plateaus  $p_1$ ,  $p_2$ , and  $p_3$  can be attributed to the confinement effect along the  $x$  and  $y$  directions (see Sec. SI of the Supplemental Material [42] for more details).

#### IV. SIDE-SURFACE-MEDIATED HYBRIDIZATION

The unique transport signatures of the axion insulator phase indicate the existence of counterpropagating currents near the top and bottom surfaces, which is confirmed by checking the spectra and the corresponding wave-function distributions shown in Figs. 2(a)–2(f). The red points correspond to the diagonal hinge states shown in Fig. 2(c), and the wave-function distributions of the blue points are opposite to that of the red points, which are mainly located at the off-diagonal hinges [Fig. 2(c)]. From the spectrum shown in Fig. 2(a), we observe that the diagonal hinge states and the off-diagonal hinge states have opposite velocities. Therefore, as shown in the inset in Fig. 2(c), it is the hinge states that establish the counterpropagating chiral currents in the axion insulator phase. Moreover, at  $k_y = 0$ , the two states couple

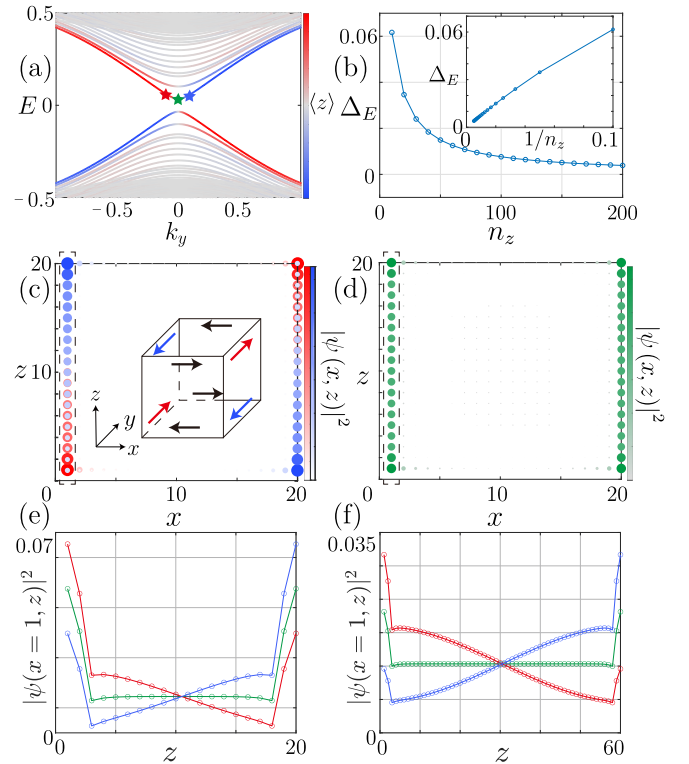


FIG. 2. (a) The spectrum of the axion insulator phase as a function of  $k_y$ . Here, the color scheme indicates the wave-function distribution shown in (c) and (d). (b) The hybridization energy gap  $\Delta_E$  at  $k_y = 0$  as a function of the film thickness  $n_z$ . The inset shows  $\Delta_E$  exhibits a linear relationship as a function of  $1/n_z$ . (e) and (f) The probability distributions  $|\psi(x=1, z)|^2$  [the area in the dashed frame in (e) and (f)] as functions of  $z$  at  $k_y = -0.01$  (red),  $k_y = 0$  (green), and  $k_y = 0.01$  (blue) with film thickness (e)  $n_z = 20$  and (f)  $n_z = 60$ , respectively. The results are calculated in the axion insulator phase with the periodic boundary condition along the  $y$  direction and the open boundary conditions along the  $x$  and  $z$  directions. The system sizes are (a), (c)–(e)  $n_x = n_z = 20$ , (b)  $n_x = 20$ , and (f)  $n_x = 20$  and  $n_z = 60$ , respectively.

together [Fig. 2(d)], and the spectrum opens a hybridization energy gap [Fig. 2(a)].

By checking the wave-function distributions, we found that hinge states are not that localized, and they can penetrate deep into the bulk. The above scenarios can be observed more clearly in Figs. 2(e) and 2(f), where we plot  $|\psi(x=1, z)|^2$  as a function of  $z$  at different  $k_y$  for different film thicknesses  $n_z$ . At  $k_y = 0$ , the wave function is uniformly distributed inside the bulk for  $3 < z < n_z - 3$ . At  $k_y \neq 0$ , the wave-function distribution  $|\psi(x=1, z)|^2$  of the surface states exhibits a linear decrease or increase as a function of  $z$ , which indicates that the top and bottom surface states are strongly hybridized.

The hybridization gap decays with increasing thickness  $n_z$  as  $\Delta_E \sim 1/n_z$  [Fig. 2(b)], which is distinct from the hybridization effect in topological insulators, where the hybridization gap exhibits an exponential decay with an increase of system size [34–37]. In fact, the counterpropagating currents are bridged by a massless Dirac fermion. As a result, the hybridization effect in axion insulators is much stronger compared to that of topological insulators, where the

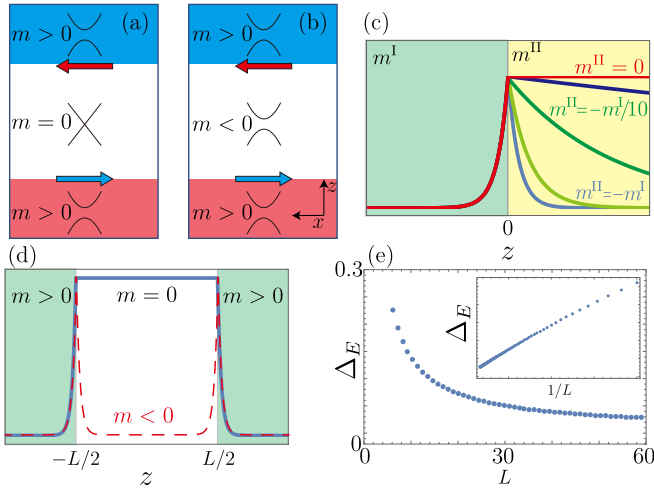


FIG. 3. (a) The side surface of the axion insulator phase can be described by a massless region sandwiched by two massive regions. (b) The topological insulator can be described by a massive region sandwiched by two massive regions. (c), (d) Probability density of the solutions in the mass domains at  $k_x = 0$ . Here, green, yellow, and white regions are characterized by different topological masses, respectively. (e) The hybridization gap  $\Delta_E$  of the solution in (d) as a function of  $L$ . We take  $m = 0.2$  in (c)–(e).

counterpropagating currents are hybridized via a fully gapped bulk [34–37].

## V. EFFECTIVE MODEL ANALYSIS

Now, we discuss the physical picture of the hybridization effect in axion insulators. Because the bulk of the magnetic topological insulator is insulating, it is effectively a closed 2D surface with six facets [16,50]. In the absence of magnetization, the effective Hamiltonian of the Dirac fermions for the surface states can be written as  $H_{\text{eff}}(\mathbf{k}) = v\hbar(\mathbf{k} \times \boldsymbol{\sigma}) \cdot \mathbf{n}$  [37,51]. The different facets have different effective Hamiltonians respective to different normal vectors  $\mathbf{n}$ . More specifically, the effective Hamiltonian can be written as  $H_{\text{vb}}^{\text{Axion}} = \pm v\hbar(k_x\sigma_y - k_y\sigma_x) \pm m\sigma_z$  for axion insulators with antiparallel magnetism on the top and bottom surfaces, respectively [57,58]. The spectra open gaps on the top and bottom facets, and the Dirac fermions gain the same mass for the axion insulator phase. Thus, the effective Hamiltonians (see Sec. SIII of the Supplemental Material [42] for more details) for the side facets can be written as  $H_{\text{side}} = v\hbar(k_x\sigma_z - k_z\sigma_x) + m(z)\sigma_z$  [16,52,59]. Here,  $m(z) > 0$  when  $z$  is near the top and bottom facets in the axion insulator, and  $m(z) = 0$  elsewhere [Fig. 3(a)].

Let us first review the famous Jackiw-Rebbi solution [60] in one dimension with the Hamiltonian  $h = -iv\hbar\partial_z\sigma_x + m(z)\sigma_z$  and  $m(z) = m^I$  for  $z < 0$  and  $m(z) = m^{II}$  for  $z > 0$ . Here, we assume  $m^I > 0$  for simplicity. For  $m^{II} = m^I$ , the system only hosts the bulk states  $E = \pm\sqrt{v^2k_z^2 + (m^I)^2}$  extending to the whole space. For  $m^{II} \leq 0$ , there exists a solution of zero energy  $E = 0$  with the corresponding wave function  $\phi(z) = C(i, 1)e^{-|m(z)z|/\hbar}$ . Hence, the wave function of the zero mode decays exponentially for  $m^{II} < 0$ , but can percolate the whole system for the massless case with  $m^{II} = 0$  [shown in Fig. 3(c)].

The axion insulator is equivalent to the 1D domain-wall structure across which the Dirac fermion mass is positive when  $z < -L/2$  and  $z > L/2$  and zero when  $-L/2 < z < L/2$  [24,25]. In the limit  $L \rightarrow 0$ , there is only the bulk state with the energy gap  $\Delta E = 2m$ . In the limit  $L \rightarrow \infty$ , the system can be regarded as two copies of the Jackiw-Rebbi system with two zero-energy modes percolating the whole system. Therefore, when  $L$  varies from  $\infty$  to zero, the energy gap of the system varies from  $2m$  to 0. The probability density of the solution is uniformly distributed in the massless region. Hence, the hybridization gap decays as  $1/L$ . The states on opposite domains are always bridged by the massless Dirac fermion [see Fig. 3(d)].

The above scenario for axion insulators [solid blue line in Fig. 3(d)] is distinct from the case of topological insulators [red dashed line in Fig. 3(d)]. The topological insulator hosts a nonzero topological mass inside the bulk. In topological insulators, the probability decays exponentially when  $z$  is away from the domain wall. Thus, the hybridization gap  $\Delta_E$  depicting the hybridization between the two domains also decays exponentially with the sample length  $L$  as  $\Delta_E \sim e^{-L}$  [34–37].

In Sec. SIII of the Supplemental Material [42], we investigate the hybridization effect in the Chern insulator phase. With an increase of the film thickness, we show that the hybridization effect is absent in the Chern insulator phase. The distinct decay patterns of the hybridization gap in the Chern and axion insulator phases explain the different transport properties shown in Figs. 1(b) and 1(f). Furthermore, in Sec. SIV of the Supplemental Material [42], we investigate the hybridization effect in a two-dimensional system with multiple topological mass domains. The above scenarios for the axion insulator phase are further confirmed.

## VI. CONCLUSION AND DISCUSSION

We study the transport signatures of the axion insulator phase in magnetic topological insulators. We show that the half-quantized counterpropagating current can be extracted in the axion insulator phase, which provides a transport signature to identify it in experiments. We argue that the shift of the conductance from half quantization can be attributed to the side-surface-mediated hybridization effect. Moreover, we reveal that the half-quantized counterpropagating current is strongly suppressed in axion insulator thin films due to the strong hybridization effect. The power-law decay of the hybridization gap manifests a different kind of finite-size effect, which can be immediately measured in experiments.

Even though the counterpropagating chiral currents in the nonlocal transport can provide signatures for the axion insulator phase, it is still hard to directly observe the resistance expected for the half-quantized counterpropagating edge current in the Hall-bar measurement of an axion insulator [27,28]. Our study shows that the hybridization effect in axion insulators can strongly suppress the half-quantized counterpropagating currents, which provides a potential mechanism to interpret the experimental result.

Besides nonlocal transport, the power-law decay of the edge-current distribution in axion insulators has been extensively studied recently [24,25]. Our findings are consistent

with the former works. In addition, we systematically investigate the strong hybridization effect exemplified by the power-law decay of the edge-current distribution and its impact on the transport properties of axion insulators.

### ACKNOWLEDGMENTS

We are thankful for helpful discussions with Bo Fu and Huan-Wen Wang. B.Z. was supported by the NSFC (under

Grant No. 12074107), the program of outstanding young and middle-aged scientific and technological innovation team of colleges and universities in Hubei Province (under Grant No. T2020001) and the innovation group project of the Natural Science Foundation of Hubei Province of China (under Grant No. 2022CFA012). H.P.S. acknowledges support by the DFG (SPP1666 and SFB1170 “ToCoTronics”), the Würzburg-Dresden Cluster of Excellence ct.qmat, EXC2147, Project-id 390858490, and the Elitenetzwerk Bayern Graduate School on “Topological Insulators”.

- 
- [1] D. Xiao, J. Jiang, J.-H. Shin, W. Wang, F. Wang, Y.-F. Zhao, C. Liu, W. Wu, M. H. W. Chan, N. Samarth, and C.-Z. Chang, Realization of the Axion Insulator State in Quantum Anomalous Hall Sandwich Heterostructures, *Phys. Rev. Lett.* **120**, 056801 (2018).
- [2] N. Varnava and D. Vanderbilt, Surfaces of axion insulators, *Phys. Rev. B* **98**, 245117 (2018).
- [3] Z. Liu and J. Wang, Anisotropic topological magnetoelectric effect in axion insulators, *Phys. Rev. B* **101**, 205130 (2020).
- [4] Y. Xu, Z. Song, Z. Wang, H. Weng, and X. Dai, Higher-Order Topology of the Axion Insulator  $\text{EuIn}_2\text{As}_2$ , *Phys. Rev. Lett.* **122**, 256402 (2019).
- [5] K. M. Fijalkowski, N. Liu, M. Hartl, M. Winnerlein, P. Mandal, A. Coschizza, A. Fothergill, S. Grauer, S. Schreyeck, K. Brunner *et al.*, Any axion insulator must be a bulk three-dimensional topological insulator, *Phys. Rev. B* **103**, 235111 (2021).
- [6] A. M. Essin, J. E. Moore, and D. Vanderbilt, Magnetoelectric Polarizability and Axion Electrodynamics in Crystalline Insulators, *Phys. Rev. Lett.* **102**, 146805 (2009).
- [7] R. S. K. Mong, A. M. Essin, and J. E. Moore, Antiferromagnetic topological insulators, *Phys. Rev. B* **81**, 245209 (2010).
- [8] C. Niu, H. Wang, N. Mao, B. Huang, Y. Mokrousov, and Y. Dai, Antiferromagnetic Topological Insulator with Nonsymmorphic Protection in Two Dimensions, *Phys. Rev. Lett.* **124**, 066401 (2020).
- [9] K. Nomura and N. Nagaosa, Surface-Quantized Anomalous Hall Current and the Magnetoelectric Effect in Magnetically Disordered Topological Insulators, *Phys. Rev. Lett.* **106**, 166802 (2011).
- [10] J. Wang, B. Lian, X.-L. Qi, and S.-C. Zhang, Quantized topological magnetoelectric effect of the zero-plateau quantum anomalous Hall state, *Phys. Rev. B* **92**, 081107(R) (2015).
- [11] T. Morimoto, A. Furusaki, and N. Nagaosa, Topological magnetoelectric effects in thin films of topological insulators, *Phys. Rev. B* **92**, 085113 (2015).
- [12] X.-L. Qi, R. Li, J. Zang, and S.-C. Zhang, Inducing a magnetic monopole with topological surface states, *Science* **323**, 1184 (2009).
- [13] J. Maciejko, X.-L. Qi, H. D. Drew, and S.-C. Zhang, Topological Quantization in Units of the Fine Structure Constant, *Phys. Rev. Lett.* **105**, 166803 (2010).
- [14] W.-K. Tse and A. H. MacDonald, Giant Magneto-Optical Kerr Effect and Universal Faraday Effect in Thin-Film Topological Insulators, *Phys. Rev. Lett.* **105**, 057401 (2010).
- [15] J. Yu, J. Zang, and C.-X. Liu, Magnetic resonance induced pseudo-electric field and giant current response in axion insulators, *Phys. Rev. B* **100**, 075303 (2019).
- [16] R.-L. Chu, J. Shi, and S.-Q. Shen, Surface edge state and half-quantized Hall conductance in topological insulators, *Phys. Rev. B* **84**, 085312 (2011).
- [17] H. Li, H. Jiang, C.-Z. Chen, and X. C. Xie, Critical Behavior and Universal Signature of an Axion Insulator State, *Phys. Rev. Lett.* **126**, 156601 (2021).
- [18] M. Mogi, Y. Okamura, M. Kawamura, R. Yoshimi, K. Yasuda, A. Tsukazaki, K. S. Takahashi, T. Morimoto, N. Nagaosa, M. Kawasaki *et al.*, Experimental signature of the parity anomaly in a semi-magnetic topological insulator, *Nat. Phys.* **18**, 390 (2022).
- [19] S. Grauer, K. M. Fijalkowski, S. Schreyeck, M. Winnerlein, K. Brunner, R. Thomale, C. Gould, and L. W. Molenkamp, Scaling of the Quantum Anomalous Hall Effect as an Indicator of Axion Electrodynamics, *Phys. Rev. Lett.* **118**, 246801 (2017).
- [20] M. Mogi, M. Kawamura, R. Yoshimi, A. Tsukazaki, Y. Kozuka, N. Shirakawa, K. S. Takahashi, M. Kawasaki, and Y. Tokura, A magnetic heterostructure of topological insulators as a candidate for an axion insulator, *Nat. Mater.* **16**, 516 (2017).
- [21] M. Mogi, M. Kawamura, A. Tsukazaki, R. Yoshimi, K. S. Takahashi, M. Kawasaki, and Y. Tokura, Tailoring tricolor structure of magnetic topological insulator for robust axion insulator, *Sci. Adv.* **3**, eaao1669 (2017).
- [22] M. Allen, Y. Cui, E. Y. Ma, M. Mogi, M. Kawamura, I. C. Fulga, D. Goldhaber-Gordon, Y. Tokura, and Z.-X. Shen, Visualization of an axion insulating state at the transition between 2 chiral quantum anomalous Hall states, *Proc. Natl. Acad. Sci. USA* **116**, 14511 (2019).
- [23] Y. Xu, I. Miotkowski, C. Liu, J. Tian, H. Nam, N. Alidoust, J. Hu, C.-K. Shih, M. Z. Hasan, and Y. P. Chen, Observation of topological surface state quantum Hall effect in an intrinsic three-dimensional topological insulator, *Nat. Phys.* **10**, 956 (2014).
- [24] M. Gong, H. Liu, H. Jiang, C.-Z. Chen, and X. C. Xie, Half-quantized helical hinge currents in axion insulators, *Natl. Sci. Rev.*, nwad025 (2023).
- [25] J.-Y. Zou, B. Fu, H.-W. Wang, Z.-A. Hu, and S.-Q. Shen, Half-quantized Hall effect and power law decay of edge-current distribution, *Phys. Rev. B* **105**, L201106 (2022).
- [26] M. Gu, J. Li, H. Sun, Y. Zhao, C. Liu, J. Liu, H. Lu, and Q. Liu, Spectral signatures of the surface anomalous Hall effect in magnetic axion insulators, *Nat. Commun.* **12**, 3524 (2021).

- [27] Y. Li, C. Liu, Y. Wang, Z. Lian, H. Li, Y. Wu, J. Zhang, and Y. Wang, Nonlocal transport and one-dimensional conduction in the axion insulator state of  $\text{MnBi}_2\text{Te}_4$ , [arXiv:2105.10390](https://arxiv.org/abs/2105.10390).
- [28] R. Chen, S. Li, H.-P. Sun, Q. Liu, Y. Zhao, H.-Z. Lu, and X. C. Xie, Using nonlocal surface transport to identify the axion insulator, *Phys. Rev. B* **103**, L241409 (2021).
- [29] C. Liu, Y. Wang, H. Li, Y. Wu, Y. Li, J. Li, K. He, Y. Xu, J. Zhang, and Y. Wang, Robust axion insulator and Chern insulator phases in a two-dimensional antiferromagnetic topological insulator, *Nat. Mater.* **19**, 522 (2020).
- [30] Y. Deng, Y. Yu, M. Z. Shi, Z. Guo, Z. Xu, J. Wang, X. H. Chen, and Y. Zhang, Quantum anomalous Hall effect in intrinsic magnetic topological insulator  $\text{MnBi}_2\text{Te}_4$ , *Science* **367**, 895 (2020).
- [31] J. Li, Y. Li, S. Du, Z. Wang, B.-L. Gu, S.-C. Zhang, K. He, W. Duan, and Y. Xu, Intrinsic magnetic topological insulators in van der Waals layered  $\text{MnBi}_2\text{Te}_4$ -family materials, *Sci. Adv.* **5**, eaaw5685 (2019).
- [32] A. Gao, Y.-F. Liu, C. Hu, J.-X. Qiu, C. Tzschaschel, B. Ghosh, S.-C. Ho, D. Bérubé, R. Chen, H. Sun *et al.*, Layer Hall effect in a 2D topological axion antiferromagnet, *Nature (London)* **595**, 521 (2021).
- [33] Y.-H. Li and R. Cheng, Identifying axion insulator by quantized magnetoelectric effect in antiferromagnetic  $\text{MnBi}_2\text{Te}_4$  tunnel junction, *Phys. Rev. Res.* **4**, L022067 (2022).
- [34] B. Zhou, H.-Z. Lu, R.-L. Chu, S.-Q. Shen, and Q. Niu, Finite Size Effects on Helical Edge States in a Quantum Spin-Hall System, *Phys. Rev. Lett.* **101**, 246807 (2008).
- [35] R. Chen and B. Zhou, Finite size effects on the helical edge states on the Lieb lattice, *Chin. Phys. B* **25**, 067204 (2016).
- [36] J. Linder, T. Yokoyama, and A. Sudbø, Anomalous finite size effects on surface states in the topological insulator  $\text{Bi}_2\text{Se}_3$ , *Phys. Rev. B* **80**, 205401 (2009).
- [37] H.-Z. Lu, W.-Y. Shan, W. Yao, Q. Niu, and S.-Q. Shen, Massive Dirac fermions and spin physics in an ultrathin film of topological insulator, *Phys. Rev. B* **81**, 115407 (2010).
- [38] H. Zhang, C.-X. Liu, X.-L. Qi, X. Dai, Z. Fang, and S.-C. Zhang, Topological insulators in  $\text{Bi}_2\text{Se}_3$ ,  $\text{Bi}_2\text{Te}_3$  and  $\text{Sb}_2\text{Te}_3$  with a single Dirac cone on the surface, *Nat. Phys.* **5**, 438 (2009).
- [39] R.-X. Zhang, F. Wu, and S. Das Sarma, Möbius Insulator and Higher-Order Topology in  $\text{MnBi}_{2n}\text{Te}_{3n+1}$ , *Phys. Rev. Lett.* **124**, 136407 (2020).
- [40] B. Fu, Z.-A. Hu, and S.-Q. Shen, Bulk-hinge correspondence and three-dimensional quantum anomalous Hall effect in second-order topological insulators, *Phys. Rev. Res.* **3**, 033177 (2021).
- [41] F. Wilczek, Two Applications of Axion Electrodynamics, *Phys. Rev. Lett.* **58**, 1799 (1987).
- [42] See Supplemental Material at <http://link.aps.org/supplemental/10.1103/PhysRevB.107.125304> for more details of the nonlocal transport for experimental realization, layer-resolved Chern number, finite-size effect in Chern insulators, and finite-size effect in 2D multiple topological mass domains.
- [43] R. Landauer, Electrical resistance of disordered one-dimensional lattices, *Philos. Mag.* **21**, 863 (1970).
- [44] M. Büttiker, Absence of backscattering in the quantum Hall effect in multiprobe conductors, *Phys. Rev. B* **38**, 9375 (1988).
- [45] D. S. Fisher and P. A. Lee, Relation between conductivity and transmission matrix, *Phys. Rev. B* **23**, 6851 (1981).
- [46] A. MacKinnon, The calculation of transport properties and density of states of disordered solids, *Z. Phys. B* **59**, 385 (1985).
- [47] G. Metalidis and P. Bruno, Green's function technique for studying electron flow in two-dimensional mesoscopic samples, *Phys. Rev. B* **72**, 235304 (2005).
- [48] A. Roth, C. Brune, H. Buhmann, L. W. Molenkamp, J. Maciejko, X.-L. Qi, and S.-C. Zhang, Nonlocal transport in the quantum spin Hall state, *Science* **325**, 294 (2009).
- [49] R. Chen, H.-P. Sun, M. Gu, C.-B. Hua, Q. Liu, H.-Z. Lu, and X. C. Xie, Layer Hall effect induced by hidden Berry curvature in antiferromagnetic insulators, *Natl. Sci. Rev.*, nwac140 (2022).
- [50] D.-H. Lee, Surface States of Topological Insulators: The Dirac Fermion in Curved Two-Dimensional Spaces, *Phys. Rev. Lett.* **103**, 196804 (2009).
- [51] W.-Y. Shan, H.-Z. Lu, and S.-Q. Shen, Effective continuous model for surface states and thin films of three-dimensional topological insulators, *New J. Phys.* **12**, 043048 (2010).
- [52] R. Yu, W. Zhang, H.-J. Zhang, S.-C. Zhang, X. Dai, and Z. Fang, Quantized anomalous Hall effect in magnetic topological insulators, *Science* **329**, 61 (2010).
- [53] P. Michetti, P. H. Penteado, J. C. Egues, and P. Recher, Helical edge states in multiple topological mass domains, *Semicond. Sci. Technol.* **27**, 124007 (2012).
- [54] A. Agarwala and V. B. Shenoy, Topological Insulators in Amorphous Systems, *Phys. Rev. Lett.* **118**, 236402 (2017).
- [55] I. Sahlberg, A. Westström, K. Pöyhönen, and T. Ojanen, Topological phase transitions in glassy quantum matter, *Phys. Rev. Res.* **2**, 013053 (2020).
- [56] X. Wu, D. Xiao, C.-Z. Chen, J. Sun, L. Zhang, M. H. W. Chan, N. Samarth, X. C. Xie, X. Lin, and C.-Z. Chang, Scaling behavior of the quantum phase transition from a quantum-anomalous-Hall insulator to an axion insulator, *Nat. Commun.* **11**, 4532 (2020).
- [57] H.-P. Sun, C.-A. Li, S.-J. Choi, S.-B. Zhang, H.-Z. Lu, and B. Trauzettel, Magnetic topological transistor exploiting layer-selective transport, [arXiv:2206.11067](https://arxiv.org/abs/2206.11067).
- [58] H.-P. Sun, C. M. Wang, S.-B. Zhang, R. Chen, Y. Zhao, C. Liu, Q. Liu, C. Chen, H.-Z. Lu, and X. C. Xie, Analytical solution for the surface states of the antiferromagnetic topological insulator  $\text{MnBi}_2\text{Te}_4$ , *Phys. Rev. B* **102**, 241406(R) (2020).
- [59] Y. Jiang, Z. Liu, and J. Wang, Unoccupied topological surface state in  $\text{MnBi}_2\text{Te}_4$ , *Phys. Rev. B* **106**, 045148 (2022).
- [60] S.-Q. Shen, *Topological Insulators* (Springer, Singapore, 2017).